Annual Review of Chaos Theory, Bifurcations and Dynamical Systems
Vol. 6, (2016) 1-29, www.arctbds.com.

On the Synchronization of Synaptically Coupled Nonlinear Oscillators: Theory and Experiment

D. C. Saha
Physics Department, Prabhu Jagatbandhu College, Kolkata-700145, India
e-mail: dolanchampasaha@gmail.com

Papri Saha
Physics Department, B. P. Poddar Institute of Management and Technology
Kolkata-700052, India
e-mail: papri.saha@gmail.com

Anirban Ray
Department of Physics, St. Xavier's College, Kolkata - 700016, India
e-mail: anirban.chaos@gmail.com

A. Roychowdhury
Department of Physics, Jadavpur University, Kolkata - 700032, India
e-mail: arc.roy@gmail.com

Abstract: Synchronization phenomena of two nonlinear oscillator systems when coupled through a memristor are analyzed exhaustively. Due to the presence of the memristor the coupling is nonlinear and very similar to a synaptic coupler. Study of such systems are now a days extremely important due to the recent thrust on neuromorphic computing which tries to replicate the principles of operation of human brain, where a series of such systems either coupled in series or in parallel are used. Here we have considered Lorenz and Hindmarsh-Rose systems in particular. They are analyzed by numerical simulations. They are also analyzed experimentally through electronic circuits. For the experimental part, the memristor is replaced with the equivalent op-amp combination. The most striking phenomenon observed is that the synchronization shows an intermittent character with respect to parameter variations due to the existence of complex basin structure with more than one attractor. Another new aspect of this type of synchronization is its sensitive dependence on initial conditions which is due to the existence of complex basin structure with more than one attractor. As such a totally new type of synchronization is observed and explored.

Keywords: Memristor, synchronization, electronic circuit, bi-parametric plot

Manuscript accepted 12 10, 2015.

1 Introduction

In 1971 [1], L. O. Chua was the first proposed that there should be a fourth circuit element other than the three known ones, resistance (R), inductance (L) and capacitance (C). This was called memristor (M) by him to indicate that it is some kind of resistor with a memory [2]. Though it was proposed long ago but only in the year 2008 [3], Hewlett-Packard announced that its fabrication has become a possibility but still not commercially viable [4]. Potential applications of such memristors span diverse fields ranging from nonvolatile memories on the nano-scale [3, 5] to modeling neural networks [6, 7]. In the mean time people have observed that all the properties of memristor can be replicated with the help of some op-amp combination [8, 9]. As such many of the studies involving memristor utilizes op-amp combination [10, 11]. Coupling such circuits in different ways [12] has become an important field of investigation. In the light of this development, it is quite justified to ascertain some important applications of such a new device. One such is the behavior of a memristor which mimic to some extent operations of biological synapses. Just like a synapse, which is essentially a programmable wire used to connect a group of neurons together, the memristor changes its resistance adaptively. Also the strength of coupling can get stronger or weaker depending on situation in actual synaptic coupling. Thus, a programmable self-adaptive weight can be modeled through memristors. As such, its applicability in neuromorphic computing is huge. Neuromorphic computation discusses the use of very-large-scale integration (VLSI) systems containing electronic analog circuits to mimic neuro-biological architectures of nervous system [13, 14]. The term neuromorphic has been used to describe analog, digital, and mixed-mode analog/digital VLSI and software systems that implement models of neural systems (for perception, motor control, or multisensory integration). This is a new interdisciplinary subject that takes inspiration from biology, physics, mathematics, computer science and electronic engineering to design artificial neural systems, such as vision systems, head-eye systems, auditory processors, and autonomous robots, whose physical architecture and design principles are based on those of biological nervous systems. Recently some researchers at Purdue presented a design for a neuromorphic chip using lateral spin valves and memristors [15] in June 2012. Another such work was done at HP Labs on Mott memristors [16, 17]. Due to this importance, a subclass of neuromorphic computing systems that focus on the use of memristors to implement neuroplasticity, has originated and they are named neuromemristive systems. It has been predicted that a neuromemristive system may replace the details of a cortical microcircuit's behavior with an abstract neural network model.

Another significant phenomenon, that has been developed in last two decades, is synchronization [18, 19] of two or more systems. Synchronization is crucially depended on the nature of the corresponding coupling. This is immensely important from the point of view of both experiment and theory. Coupling between same variable of two or more non-linear system leads to synchronization is a well documented fact. This has been observed in many physical [20, 21], chemical [22], ecological [23, 24] and biological systems [25]. Later, this phenomena have found one of its many applications in cryptography and secure communications. Moreover, coupling nonlinear systems in different spatial configurations leads to the construction of spatiotemporal systems that can exhibit a variety of exotic dynamical behavior such as pattern formation, wave propagation, rotating spirals

[26] and chimera. They mimic spatiotemporal dynamics, observed in biological systems [27], very well. Finally, recent works have shown that coupling nonlinear elements can invoke a plethora of interesting phenomena, such as hysteresis, phase locking, phase shifting, phase flip, amplitude death [28, 29, 30] and oscillation death [31] in the dynamical behavior of the coupled systems.

So our motivation in the present communication is to bring the two field together. Thus, we analyze the behavior of two non-linear oscillators coupled though a memristor. At first system, we have taken two Lorenz systems [32] and then we have used two Hindmarsh-Rose oscillators [33]. There have been various discussions on coupled Lorenz or Hindmarsh-Rose system to study the process of synchronization [18]. But these are essentially linear one way or two way coupling. But the memristor itself is not a linear device as such the coupling itself is nonlinear. To ascertain the various aspects of such a new analysis we have studied the problem both from the theoretical and experimental view point. An electronic circuit is constructed with the help of operational amplifier to simulate the behavior of a memristor, which is then used to connect the circuits for two Lorenz or two Hindmarsh-Rose circuits. All the results related to the chaotic and periodic behavior, synchronization, bifurcation are obtained from both these approaches and are seen to corroborate each other. Important features of this type of synchronization procedure are;

(a) The process is intermittent with respect to parameter variation. An event not so well known but may be ascribed to the existence of more than one attractor. Standard intermittency is with respect to time which is usually observed during the time of synchronization.

(b) The process is highly sensitive to the change in the initial condition difference, which is an outcome of multi-stable error equation. This is an effect of coupled system becoming a multi-attractor system.

(c) These new kind of events may have been triggered due to the existence of line of fixed points in the coupled system due to the fact that the flux variable of memristor do not posses any fixed value.

Hindmarsh-Rose (HR) model of neuronal activity is aimed to simulate spiking-bursting behavior of the membrane potentials observed in a single neuron. Thus, our choice of using Hindmarsh-Rose (HR) oscillator for synchronization is driven by our aim of using memristor in neural modeling.

2 Formulation

2.1 Lorenz Equation

Suppose x components of the two Lorenz equations (i.e., (x_1, x_2) are variables) are coupled via a memristor, whose flux variable is 'u'. Thus the equation governing two Lorenz system

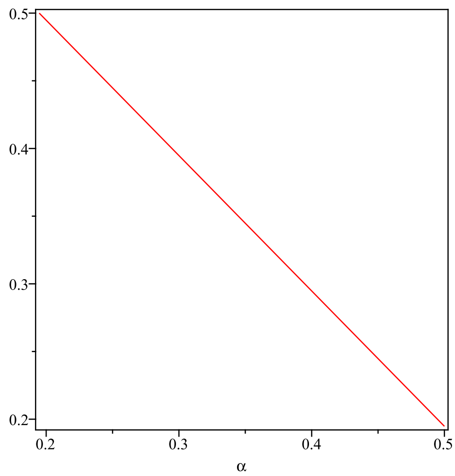

Figure 1: Stability diagram in (α, β) space where u is kept at 1.

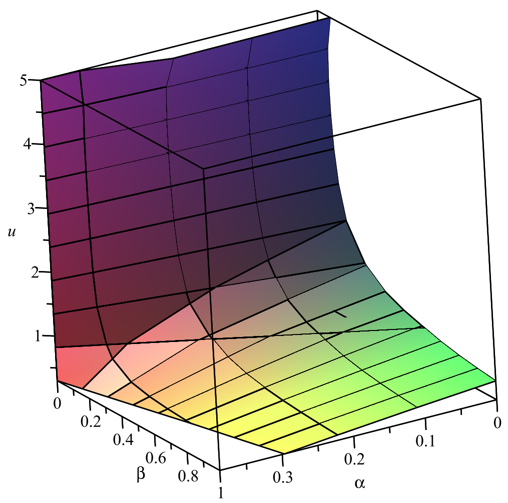

Figure 2: Three dimensional figure in (α, β, u) space of eigenvalue.

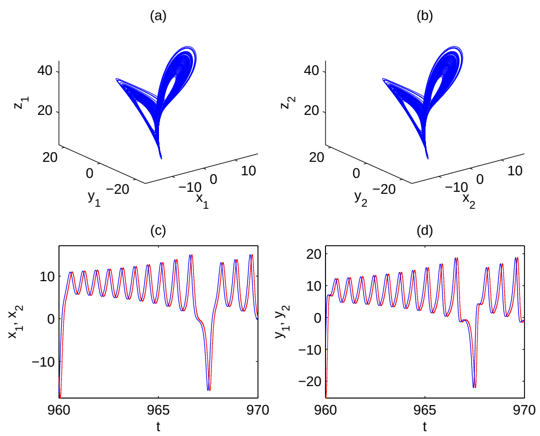

Figure 3: Phase synchronization between two sets of Lorenz equations represented in Eq. (1). Parameter values are kept at $c = 0.1$, $\alpha = 0.2$, and $\beta = 0.4$. Here (a) and (b) represent two attractors while (c) represent the two time series x_1 and x_2.

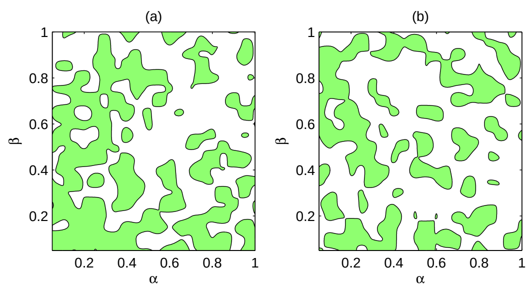

Figure 4: Parameter region indicating phase synchronization on (α, β) plane. Figure (a) is plotted for $c = 0.1$ and figure (b) is plotted for $c = 0.2$. Other parameter values are kept at $\sigma = 10,\ r = 28$ and $b = \frac{8}{3}$.

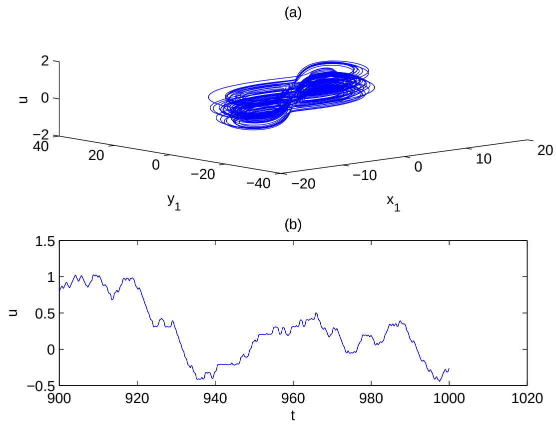

Figure 5: Phase space structure in (x_1, y_1, u) space is shown in Fig. (a) and time series of u is shown in Fig. (b). These situations are plotted for $c = 0.01$ i.e., the situations when synchronization is not archived. Other parameter values are kept at $\sigma = 10$, $r = 28$ and $b = \frac{8}{3}$.

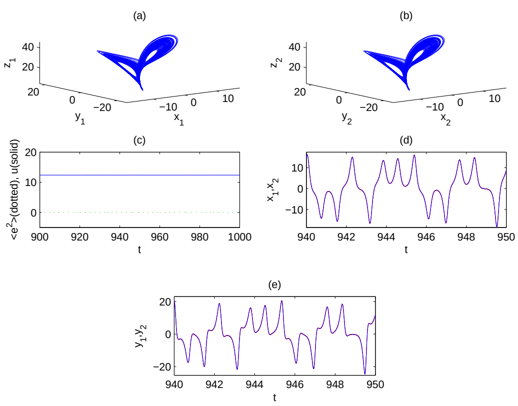

Figure 6: Time series of Lorenz system at complete synchronization. Parameter values are kept at $c = 0.5$, $\alpha = 0.2$, and$\beta = 0.4$. Here (a) and (b) represent two attractors. (c) represent mean squared value of error $< e^2(t) >$ with time and u with time. (d) represent the two time series x_1 and x_2. (e) represent the two time series y_1 and y_2.

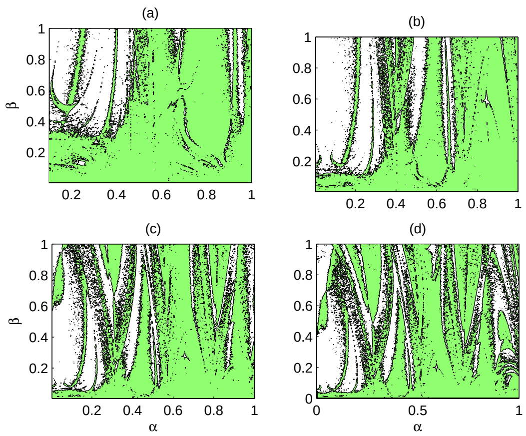

Figure 7: Parameter region indicating complete synchronization on (α, β) plane. Figure (a) is plotted for $c = 0.5$, figure (b) is plotted for $c = 0.7$, figure (c) is plotted for $c = 0.9$ and figure (d) is plotted for $c = 1.0$. Other parameter values are kept at $\sigma = 10,\ r = 28$ and $b = \frac{8}{3}$. Initial errors are $e_x(0) = 0.1,\ e_y(0) = 0.1 \text{and} e_z(0) = 0.1$.

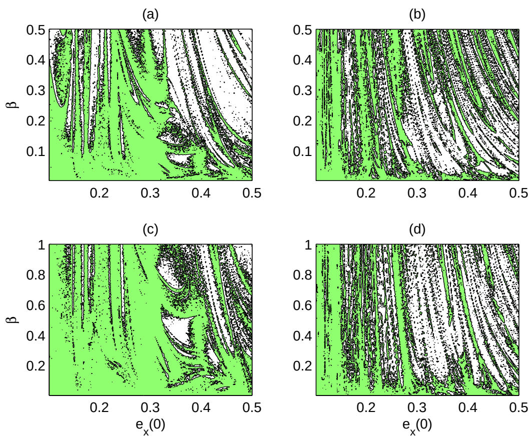

Figure 8: Parameter region indicating complete synchronization on $(e_x(0), \beta)$ plane. Figure (a) is plotted for $c = 0.5$, figure (b) is plotted for $c = 0.7$, figure (c) is plotted for $c = 0.9$ and figure (d) is plotted for $c = 1.0$. Other parameter values are kept at $\sigma = 10,\ r = 28,\ b = \frac{8}{3}$and $\alpha = 0.4$.

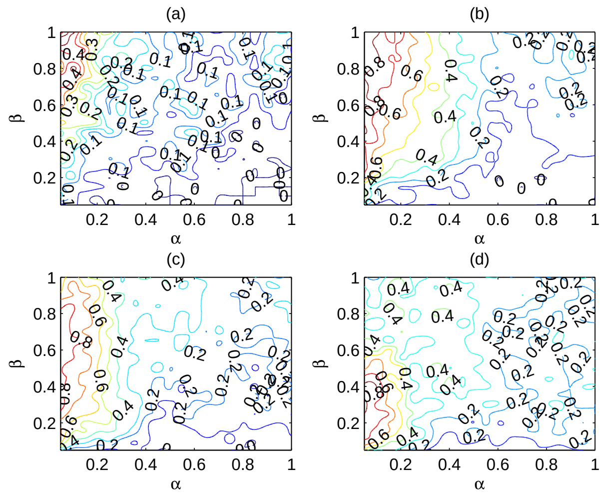

Figure 9: Parameter region indicating fraction of initial condition combination that reaches synchronization for a particular value of coupling 'c' on (α, β) plane. Fig. (a) is plotted for $c = 0.3$, Fig. (b) is plotted for $c = 0.6$, Fig. (c) is plotted for $c = 0.8$ and Fig. (d) is plotted for $c = 1.0$. Other parameter values are kept at $\sigma = 10$, $r = 28$ and $b = \frac{8}{3}$.

[32] coupled through a memristor can be written as

$$\begin{aligned}
\dot{x}_1 &= \sigma(y_1 - x_1) + c(\alpha + \beta u^2)(x_2 - x_1) && \text{(1a)}\\
\dot{y}_1 &= r x_1 - y_1 - x_1 z_1 && \text{(1b)}\\
\dot{z}_1 &= x_1 y_1 - b z_1 && \text{(1c)}\\
\dot{x}_2 &= \sigma(y_2 - x_2) + c(\alpha + \beta u^2)(x_1 - x_2) && \text{(1d)}\\
\dot{y}_2 &= r x_2 - y_2 - x_2 z_2 && \text{(1e)}\\
\dot{z}_2 &= x_2 y_2 - b z_2 && \text{(1f)}\\
\dot{u} &= c(x_2 - x_1) && \text{(1g)}
\end{aligned}$$

where the memristor is an electronic element which satisfies the following equation

$$\begin{aligned}
W(u) &= \frac{dq(u)}{du} && \text{(2a)}\\
i_M &= W(u) V_M && \text{(2b)}
\end{aligned}$$

Here, $W(u)$ is called memductance. The associated current is i_M and voltage is V_M. The current and voltage are related through Eq. (2). At present various forms of memductance are in use of which a cubic from is most popular. So here we consider flux controlled memristor with cubic $q(u)$.

It is apparent from the above equations the 'x' components of the two Lorenz equations are connected via the memristor which is of standard cubic type initially suggested by Leon O. Chua.

$$q(u) = \alpha u + \frac{\beta}{3} u^3 \tag{3}$$

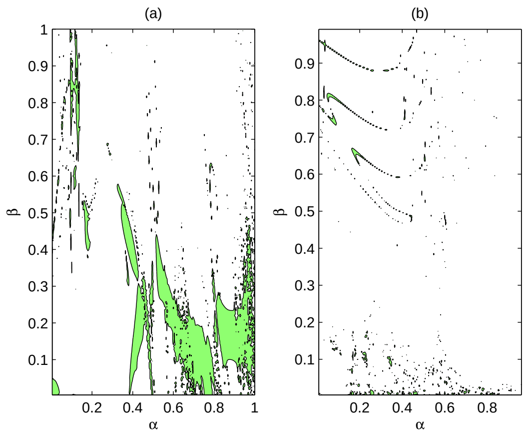

Figure 10: Parameter region indicating phase synchronization on (α, β) plane. Figure (a) is plotted for $c = 0.001$ and figure (b) is plotted for $c = 0.01$. Other parameter values are kept at $a = 3.0,\ b = 5.0,\ I = 3.05,\ s = 4.0,\ c_0 = 1.6$ and $r = 0.005$.

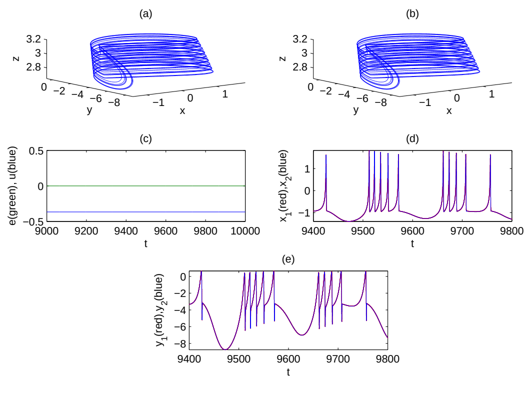

Figure 11: Time series of HR system at complete synchronization. Parameter values are kept at $c = 0.5$, $\alpha = 0.2$, and$\beta = 0.4$. Here (a) and (b) represent two attractors. (c) represent mean squared value of error $< e^2(t) >$ with time and u with time. (d) represent the two time series x_1 and x_2. (e) represent the two time series y_1 and y_2.

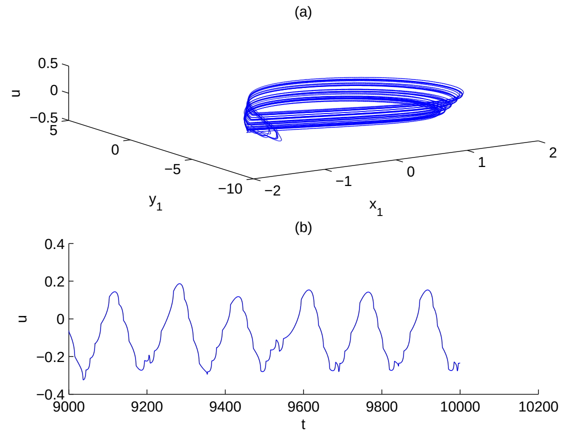

Figure 12: Phase space structure in (x_1, y_1, u) space is shown in Fig. (a) and time series of u is shown in Fig. (b). These situations are plotted for $c = 0.01$ i.e., the situations when synchronization is not archived. Other parameter values are kept at $a = 3.0,\ b = 5.0,\ I = 3.05,\ s = 4.0,\ c_0 = 1.6$ and $r = 0.005$.

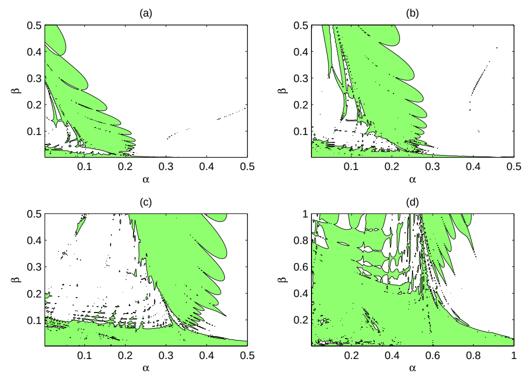

Figure 13: Parameter region indicating complete synchronization of two Hindmarsh-Rose systems on (α, β) plane. Figure (a) is plotted for $c = 0.3$, figure (b) is plotted for $c = 0.5$, figure (c) is plotted for $c = 0.7$ and figure (d) is plotted for $c = 0.9$. Other parameter values are kept at $a = 3.0,\ b = 5.0,\ I = 3.05,\ s = 4.0,\ c_0 = 1.6$ and $r = 0.005$. Initial errors are $e_x(0) = 0.1,\ e_y(0) = 0.1$ and $e_z(0) = 0.1$.

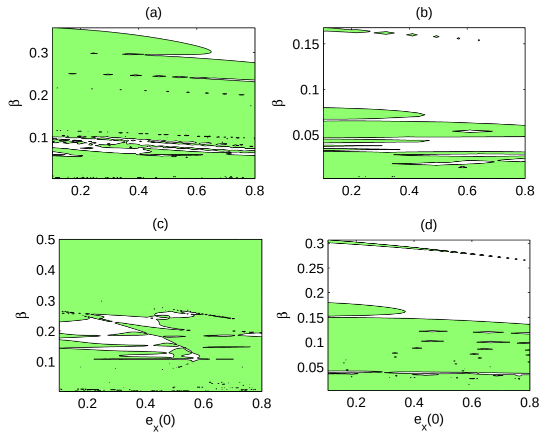

Figure 14: Parameter region indicating complete synchronization of two Hindmarsh-Rose systems on $(e_x(0), \beta)$ plane. Figure (a) is plotted for $c = 0.3$, figure (b) is plotted for $c = 0.5$, figure (c) is plotted for $c = 0.7$ and figure (d) is plotted for $c = 0.9$. Other parameter values are kept at $a = 3.0,\ b = 5.0,\ I = 3.05,\ s = 4.0,\ c_0 = 1.6\ \ r = 0.005,$ and $\alpha = 0.1$.

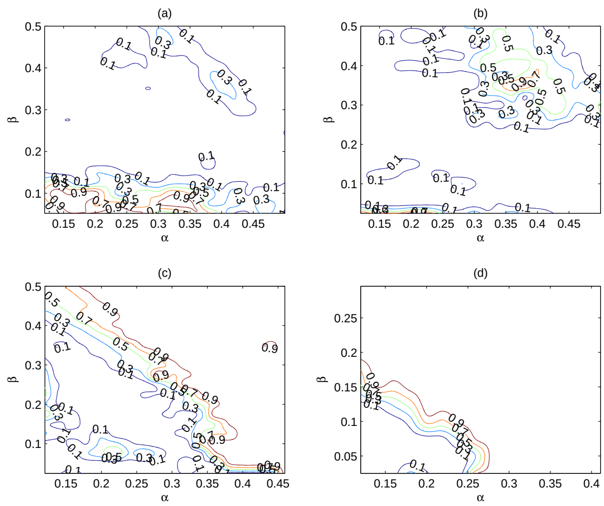

Figure 15: Parameter region indicating fraction of initial condition combination that reaches synchronization for a particular value of coupling 'c' on (α, β) plane. Fig. (a) is plotted for $c = 0.2$, Fig. (b) is plotted for $c = 0.3$, Fig. (c) is plotted for $c = 0.5$ and Fig. (d) is plotted for $c = 0.7$. Other parameter values are kept at $a = 3.0,\ b = 5.0,\ I = 3.05,\ s = 4.0,\ c_0 = 1.6\ \ r = 0.005,$ and $\alpha = 0.1$.

Substituting eq. (3) in eq. (2), we get the following relation

$$i_M = (\alpha + \beta u^2)V_M \tag{4}$$

This expression contributes the coupling term in Eqs. (1a) and(1d). Now, the fixed points of the system are $x_1 = x_2 = 0$, $y_1 = y_2 = 0$, $z_1 = z_2 = 0$ for arbitrary 'u', or for $x_{1,2} = y_{1,2} = \pm\sqrt{br - b}$, and $z_{1,2} = r - 1$ again for arbitrary 'u'. Hence the system has a line of equilibria contained in the 'u'-axis. The linearized system around the first fixed point has the eigenvalues, $\{0, -\frac{1}{2} - \frac{1}{2}\sigma + M, -\frac{1}{2} - \frac{1}{2}\sigma - M, -\beta cu^2 - \alpha c - \frac{1+\sigma}{2} + \frac{1}{2}N, -\beta Cu^2 - \alpha c - \frac{1+\sigma}{2} - \frac{1}{2}N, -b, -b\}$ where M and N are given as

$$\begin{aligned} M &= \sqrt{4r\sigma + \sigma^2 - 2\sigma + 1} \\ N &= [4\beta^2c^2u^4 + 8\alpha\beta c^2u^2 + 4\beta c\sigma u^2 + 4\alpha^2c^2 - 4\beta cu^2 \\ &\quad +4\alpha c\sigma - 4\alpha c\sigma - 4\alpha c + 4r\sigma + \sigma^2 - 2\sigma + 1]^{\frac{1}{2}} \end{aligned}$$

On the other hand for the fixed point $x_1 = y_1 = \sqrt{br - b}, z_1 = z_2 = r - 1, x_2 = y_2 = \sqrt{br - b}$, real part of the eigen value is is shown in Fig. (1). It shows variation within (α, β) plane. The eigenvalue equation can be factorized as

$$\begin{aligned} &\frac{1}{9}\{3\lambda^3 + 41\lambda^2 + 304\lambda + 4320 + b\lambda^2 c\beta u^2 \\ &+22\lambda c\beta u^2 + 448c\beta u^2 + b\lambda^2 c\alpha + 22\lambda c\alpha + 448c\alpha\} \\ &\{3\lambda^3 + 41\lambda^2 + 30\lambda + 4320\} = 0 \end{aligned} \tag{5}$$

As evident from eigenvalues that stability of the coupled system does not depend on sign of 'u'. Through out the rest of the paper, we have assumed, $\sigma = 10$, $r = 28$ and $b = \frac{8}{3}$. The onset of instability can be ascertained with the help of Routh stability criterion. In this connection, one should note that we have assumed u to be arbitrary in our above computation till now. To ascertain the stability of the system from change of sign of the eigen value with variation of α andβ, we must fix the value of u. If we fix $u = 1$, then eigen values give an implicit relation of (α, β), which is simply a straight line as evident from Fig. (1). Region below the straight line is stable and region above this straight line is unstable. If we vary u from 0.0 to 5.0, we get the figure given in Fig. (2). The plane represent the combination of values of α, β and u for which chaotic motions set in. Fig. (2) indicates that the region in (α, β) plane where chaos sets in decreases with the increment of values of 'u' above '1'. Opposite phenomena happens, if we decrease it below '1'. From calculation of coefficients of the Routh table above conditions for instability can be crosschecked. First we identify, inphase synchronization between two Lorenz system coupled through the procedure described in Eq. (1). Fig. (3) depicts a situation when two coupled Lorenz systems are inphase. There we have taken $c = 0.1$, $\alpha = 0.2$, and $\beta = 0.4$. Here coupled systems are kept at slight parameter mismatched conditions(we kept $\sigma = 10$ for first system and $\sigma = 10.1$ for second system). In Fig. (3a) and (3) we show the structure of the attractors. Onset of phase synchronization is identified with the help of Lyapunov exponents(λ_i, where $i = 1, \cdots, 7$) of the coupled system. Inphase synchronization sets in as the fourth largest Lyapunov exponent(λ_4) becomes negative from zero [34]. The region of phase synchronization in (α, β) plane are denoted in Fig. (4). These figures are obtained by denoting points where fourth maximum Lyapunov exponent (λ_4) of the coupled system crosses from zero to negative value. Regions of phase synchronization are identified through white space and non-phase synchronizing regions are identified with green color. Figs. (4a) and (4b) show two such scenarios for two different coupling values $c = 0.1$ and $c = 0.2$ respectively. Intermittency in parameter region depicting onset of phase synchronization in (α, β) plane is evident from both Figs. (4a) and (4b). Here 'intermittency' denotes the island like structures in (α, β) plane denoting values of (α, β) for which inphase synchronization occur in the coupled system.

Next, we have tried to identify identical synchronization between two memristively coupled Lorenz systems. In Fig. (5a), we exhibit the three dimensional projection of the memristive Lorenz equation in the (u, x, y) space. This figure suggest that in-spite of the structure of the Eq. (1) the variable 'u' remains bounded and the projected phase space has an attractor structure, which is verified by the computation of Lyapunov exponents. Fig. (5b) shows that time series of $'u'$. Both of this figures are plotted when synchronization is not archived. A similar analysis can also be done for the Hindmarsh-Rose equation. To start with, we initially investigate the occurrence of phase synchronization. We depict one such scenario in Fig. (6) i.e., situation when memristively coupled Lorenz systems are identically synchronized. We show two individual attractors in Figs. (6a) and (6b), where as the corresponding time series (x_1, x_2) and (y_1, y_2) are shown in (6d) and (6e). The expected values of the square of the error tending towards zero at synchronization is shown in Fig. (6c) and value of u, when synchronization occur, is measured as $u = 11.2$. So it is concluded that the two Lorenz systems synchronize when they are being coupled through a memristor. We now proceed to verify the existence of complete synchronization by the computation of Lyapunov exponents of the coupled system. We identify the complete synchronization when second largest Lyapunov exponent(λ_2) crosses zero from being positive.

In Fig. (4), we exhibit regions of synchronization for the coupled Lorenz systems of Eq. (1) by computing zero crossing of second largest Lyapunov exponent(λ_2). Synchronizing regions are indicated with white color on (α, β) plane for a fixed values of coupling constant 'c' and asynchronous regions are identified with green. It is interesting to note that these regions are intermixed and scattered over the whole region of (α, β) plane under the purview of this numerical investigation. This indicates that the synchronization stat does not exist continuously after its first occurrence on (α, β) plane, but some times gets lost. So this is called intermittent synchronization, with respect to the variation of parameter values(as they exist intermittently on (α, β) plane), not with respect to time. For a better understanding of the situation, we have calculated variation of zero crossing of second largest Lyapunov exponent with respect to parameters (α, β) for different values of 'c'. These are depicted in Fig. (7a) to (7d) for coupling values $c = 0.5, c = 0.7, c = 0.9$ and $c = 1.0$ respectively. In each case green and white regions indicate asynchronous and synchronous states respectively. All these figures are plotted with initial error values $e_x(0) = e_y(0) = e_z(0) = 0.1$ where these errors are defined as $e_x(0) = x_2(0) - x_1(0)$, $e_y(0) = y_2(0) - y_1(0)$, $e_z(0) = z_2(0) - z_1(0)$. Initial point of the first system of are kept at values $x_1(0) = 0.1$, $y_1(0) = 0.2$, $z_1(0) = 0.3$. These initial conditions are kept fixed through out the paper. Values of $(x_2(0), y_2(0), z_2(0))$ are varied according to the value of $(e_x(0), e_y(0), e_z(0))$. These scheme is used for all simulations in this paper. The importance of stating the initial values will be explained later. These figures indicate intermittent occurring of complete synchronization in parameter space of $(\alpha,\ \beta)$.

A further peculiarity of the system is described in Figs. (8a) to (8d), where we have kept $\alpha = 0.3$ constant and we have varied β along with initial error between the two systems along x direction $e_x(0)$, for coupling values $c = 0.5, c = 0.7, c = 0.9$ and $c = 1.0$ respectively. Fig. (8) indicates a strong intermittent behavior with respect to the initial value difference of coupled system. This is occurring as the corresponding error equations have line of fixed points($e_x = 0, e_y = 0, e_z = 0$, and arbitrary values of 'u'). Such a situation has not been seen before and this is actually an effect of the memristive coupling. We have studied effects of initial differences($e(0) = (e_x(0), e_y(0), e_z(0))$) in initial conditions of coupled Lorenz system through memristor in Figs. (24). Here we have calculated the fraction(F_s) of total initial condition differences between two coupled Lorenz circuits that leads to synchronization over total number of initial condition difference combination taken for calculation. Here F_s is defined as number(n_s) of combination of initial condition difference between coupled Lorenz system for which synchronization can be archived over total number(n) of such combinations taken for calculation(i.e., $F_s = \frac{n_s}{n}$). For that we have varied $e_x(0)$, $e_y(0)$ and $e_z(0)$ between '$0'$ and '$1'$ continuously in a $100 \times 100 \times 100$ combination. Then we have calculated the fraction of initial conditions for which second maximum Lyapunov exponent (λ_2) becomes negative over total number of initial difference taken. Figs. (24a), (24b), (24c) and (24d) show the contour lines (i.e., isolines) indicating fraction values (F_s) from 0.0 to 1.0. Here, $F_s = 0.2$ indicates that only 20% of initial condition difference combinations can lead to synchronization over total number of combinations where as $F_s = 0.8$ indicates 80% of initial condition difference combinations can lead to synchronization over total number of combinations. Value of 'c' is increased from 0.3 to 1.0 as we go from Fig. (24a) to Figs. (24d). If we look at them minutely, then one can identify that with the increase of 'c' fraction (F_s)) of initial condition difference combination going towards synchronization show increment in the left zone of figures. As value of 'c' crosses 1.0 this increment subsides. We have shown four such situations in Figs. (24). A detailed transition is shown in the appendix.

2.2 Hindmarsh-Rose Equation

The Hindmarsh-Rose equation is actually a nonlinear dynamical system which describes the pulse propagation in neurons, and is very important from biophysical perspective.

Here two such equations are coupled through a memristor.

$$\dot{x}_1 = y_1 + ax_1^2 - x_1^3 - z_1 + I + c(\alpha + \beta u^2)(x_2 - x_1) \quad (6a)$$
$$\dot{y}_1 = 1 - bx_1^2 - y_1 \quad (6b)$$
$$\dot{z}_1 = -rz_1 + sr(x_1 + c_0) \quad (6c)$$
$$\dot{x}_2 = y_2 + ax_2^2 - x_2^3 - z_2 + I + c(\alpha + \beta u^2)(x_1 - x_2) \quad (6d)$$
$$\dot{y}_2 = 1 - bx_2^2 - y_2 \quad (6e)$$
$$\dot{z}_2 = -rz_2 + sr(x_2 + c_0) \quad (6f)$$
$$\dot{u} = c(x_2 - x_1) \quad (6g)$$

The analysis is too complicated to be followed analytically, so only numerical simulations are given. But the numerical results show same interesting phenomena that have already been described in previous section. Before describing in-phase synchronization, we have shown the phase space structure and time series of u in Fig. (12). This the situation of of that system when synchronization is not archived for Hindmarsh rose systems. We have employed previously described method of finding inphase synchronization in terms of fourth maximum Lyapunov exponent (λ_4) of the coupled system. We have calculated the value of fourth maximum Lyapunov exponent (λ_4) of the coupled system and have studied its variations from zero to negative value on (α, β) plane to find regions where inphase synchronization occurs. The variation of λ_4 is shown in Fig. (10a) and (10b) for the choice of coupling $c = 0.001$ and $c = 0.01$ respectively. In Fig. (10a) and (10b), the region of inphase synchronization is depicted with white where as green represents the region where inphase synchronization cannot occur. In each case, variation of fourth maximum Lyapunov exponent (λ_4)) on (α, β) plane for fixed values of 'c' clearly suggest an intermittent character of inphase synchronization in the sense described in previous section. Then we analyze the complete synchronization of memristively coupled Hindmarsh-Rose systems.

An example of complete synchronization is depicted in Fig. (11). We show three dimensional projection of individual system's attractor in Fig. (11a) and (11b). The time series (x_1, x_2) and (y_1, y_2) are given in Fig. (11d) and (11e). But the error is given in Fig. (11c) where value of u saturates to $u = -0.39$, which shows that a state of synchronization has been archived. In each of these figures we have set $c = 0.5$, $\alpha = 0.2$, and $\beta = 0.4$. Initial condition differences are kept at $e_x(0) = 0.1$, $e_y(0) = 0.25$ and $e_z(0) = 0.4$ where these errors are defined as $e_x(0) = x_2(0) - x_1(0)$, $e_y(0) = y_2(0) - y_1(0)$, $e_z(0) = z_2(0) - z_1(0)$. To have a better understanding of complete synchronization, we have also calculated values in (α, β) when second maximum Lyapunov exponent(λ_2) changes from positive to negative and this is shown in Fig. (13a) to Fig. (13d) for various values of 'c'(as it is stated in previous section when second maximum Lyapunov exponent(λ_2) crosses from positive to negative through zero, complete synchronization occurs in the coupled system). Values of 'c' for different Figs. (13a),(13b),(13c) and (13d) are given as $c = 0.3$, $c = 0.5$, $c = 0.7$ and $c = 0.9$. Here also green regions describe states where complete synchronization cannot occur and white regions describe regions where complete synchronization can occur. In green regions of Fig. (13) second maximum Lyapunov exponent(λ_2) is positive and second maximum Lyapunov exponent(λ_2) is negative in white regions. It is important to note that the region of synchronization and desynchronization drastically changes with variation of coupling. In the next stage, we have kept 'c' and α fixed but have varied β and the initial difference of the two system along x-direction i.e., $e_x(0) = x_2(0) - x_1(0)$. The corresponding situations are depicted in Fig. (14). α is kept fixed at 0.1 for all figures in Fig. (14). Values of 'c' corresponding to Figs. (14a), (14b), (14c) and (14d) are $c = 0.3$, $c = 0.5$, $c = 0.7$ and $c = 0.9$ respectively. Again one should note that the intermittent character arising from multistability of the error equation is evident in these figures as we find different islands of synchronization denoted through white region in figures. Like the previous example, we then simulate the system with $100 \times 100 \times 100$ combinations of $e_x(0) = x_2(0) - x_1(0)$, $e_y(0) = y_2(0) - y_1(0)$ and $e_z(0) = x_2(0) - x_1(0)$ lying between 0 and 1. Fraction(F_s) of initial value difference combination(n_s) for which coupled system goes to synchronization over total number of combinations taken(n_s)) are represented in Fig. (25). These are calculated using the method used in previous section for Lorenz system. Values of 'c' for different Figs. (25a),(25b),(25c) and (25d) are given as $c = 0.2$, $c = 0.3$, $c = 0.5$ and$c = 0.7$. Here also we see an anomalous behavior of fraction F_s. For lower value of 'c', most of the initial condition difference leads to chaos synchronization for lower values of α and β and this fractional value F_s (i.e., fraction of initial condition difference that reaches synchronization) decreases with increasing value of α and β. This is evident from $\alpha > 0.4$ and $\beta > 0.4$ region in Fig. (25a). As value of 'c' increases this fraction of initial condition difference that reaches synchronization requires higher value of α and β. For lower values of α and β, fractions values are close to zero(this is evident in Figs. (25b),(25c) and (25d)). Thus, a flipping transition in region depicting maximum value of fraction F_s on (α, β) plane occurs as we increase coupling value 'c'. A detailed transition is shown in the appendix where this flipping is more prominent.

3 Experimental Simulation

The analogue circuit pertaining to the Lorenz equation [35] is well known and the two circuits Lorenz1 and Lorenz2 are shown in Fig. (16). Each Lorenz circuit consists of two high speed multipliers AD633 and one quad-core OP-amps TL084CN with three ceramic capacitors of 0.01 μF and resistance of varying degree of ohms from 10k to 100k, with a power source of 12 V. The circuit shown in the middle of the Fig. (16) is the coupling which actually consists of three parts. First part is the voltage divider, then an amplifier and last part is a voltage inverter. The amplifier part consist of a memristor and a feedback resistance. This is actually responsible for the coupling term in the second equation in (1). As the exact hardware for the memristor is still not commercially available the memristor is represented with the help of circuit shown in Fig. (17), which consists of two AD633 along with one TL084CN Op-amp, a ceramic capacitor, resistance and voltage source. Before going into the detail of results obtained from this circuit, let us describe the the individual Lorenz circuit and memristor circuit in detail. To model the Lorenz system, we have to scale the variables $(x,\ y,\ z)$ within the active voltage range.

$$u_{1,2} = \frac{x_{1,2}}{\sqrt{aR}},\ v_{1,2} = \frac{y_{1,2}}{\sqrt{aR}} \text{ and } w_{1,2} = \frac{z_{1,2}}{aR}$$

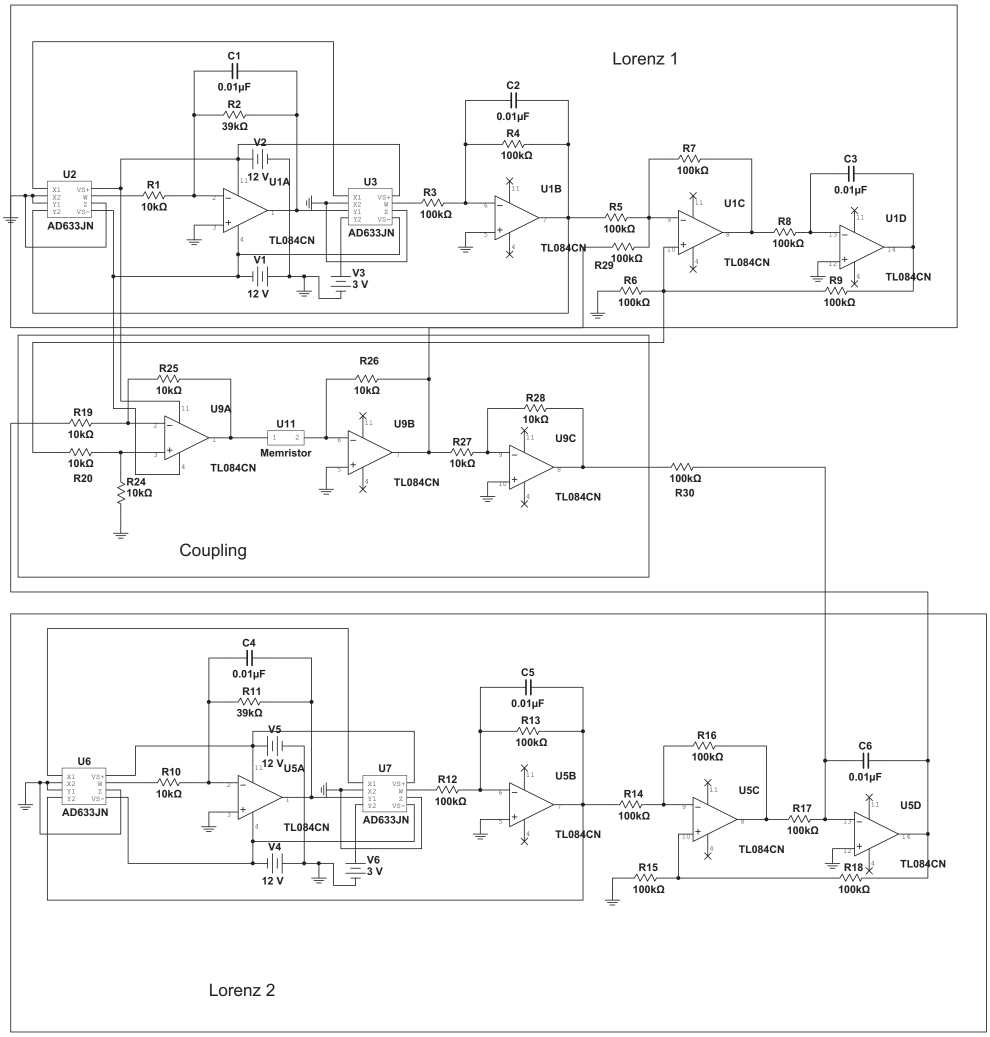

Figure 16: Two coupled electronic Lorenz circuits

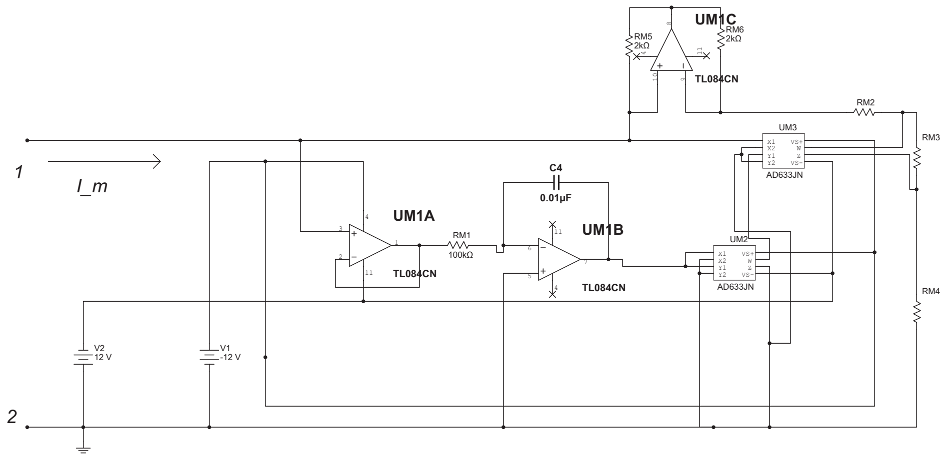

Figure 17: Memristor implementation through Op-amp combination

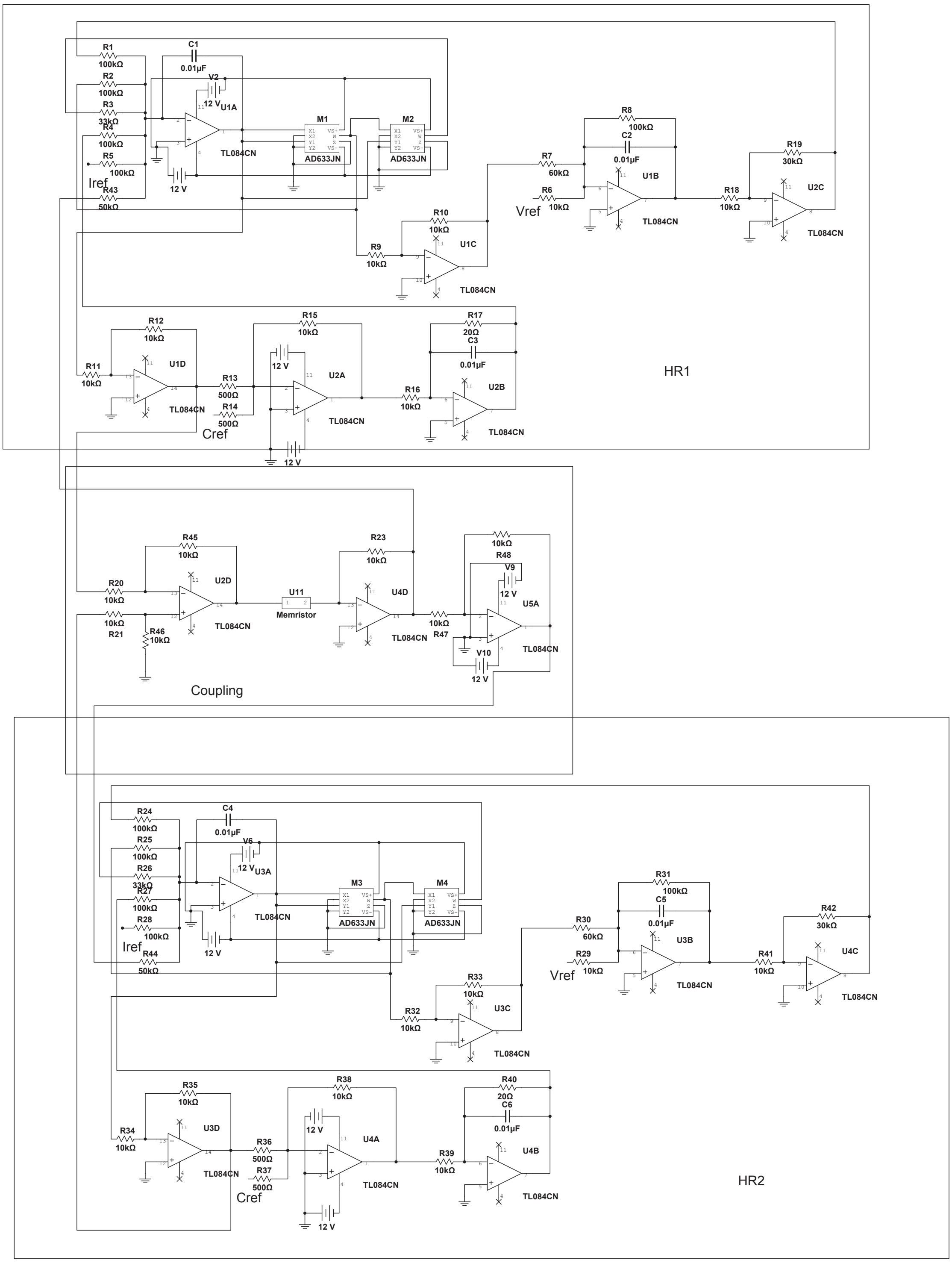

Figure 18: Two coupled electronic Hindmarsh-Rose circuits

We have taken $a = \frac{1}{3}$. Then three oscillator parameters (σ, R and b) are controlled by three resistors of each Lorenz circuit. They are given bellow.

$$\sigma = \frac{100k}{R_8} = \frac{100k}{R_{17}},\ R = \frac{10k}{R_3} = \frac{10k}{R_{12}} \text{ and } b = \frac{100k}{R_2} = \frac{100k}{R_{11}}$$

Now we describe the memristor circuit given in Fig. (17). Here, Op-amp UM1A acts as buffer and Op-amp UM1B acts in integrator mode whose output is $v_{15} = -\frac{1}{RM_1 CM_4}\int v_1 d\tau$. In Fig. (17), we can see that multiplier UM2 implements:

$$v_{UM2}(t) = -\frac{v_{15}^2}{10} \tag{7}$$

The factor of 10 is inherent to the AD633 and we refer to its datasheet for further information. Multiplier UM3 in Fig. (17) implements

$$v_{UM3}(t) = v_{UM2}(t)\left(\frac{RM_3 + RM_4}{10RM_3}\right) \tag{8}$$

Op-amp UM1C in Fig. (17) is the current inverter that implements (when $RM5 = RM6$):

$$i_m = \frac{-v_1(t)}{RM_2} + \frac{v_{UM3}(t)}{RM_2} \tag{9}$$

Substituting for $v_{UM2}(t)$ from Eq. (7) into Eq. (8) and then substituting the result into Eq. (9) we get,

$$i_m = \left(-\frac{1}{RM_2} - v_{15}^2\left(\frac{RM_3 + RM_4}{100RM_3RM_2}\right)\right).v_1 \tag{10}$$

Then the output of the amplifier in the coupler circuit becomes

$$v_{out} = R_{26}\left(\frac{1}{RM_2} + v_{15}^2\left(\frac{RM_3 + RM_4}{100RM_3RM_2}\right)\right).v_1 \tag{11}$$

Thus, the memductance parameter are changed using relations $\alpha = \frac{1}{RM_2}$ and $\beta = \left(\frac{RM_3+RM_4}{100RM_3RM_2}\right)$. The coupling constant 'c' is changed using the relation $c = \frac{R_{22}}{R_{19}}$. Here we have kept $R_{20} = R_{19}$ and $R_{25} = R_{24}$. The output from these two Lorenz circuits are fed into an oscilloscope and results are shown in Fig. (19a) and Fig. (19b). The individual time series are seen in Fig. (19d) where as the variation of x_1 with x_2 is seen in Fig. (19c) which is seen to be a simple, straight line. This indicate that the two signals are almost same or synchronized. Later, the whole arrangement is connected via one $NIUSB - 6363DAQ$ (32 AI Channels (16 BNC), 2 MS/s) to a computer to acquire the data generated by electronic circuit for further analysis. As the circuit uses resistance with 5% tolerance, a bit of trial and error goes before taking the actual data for bringing the two circuits to the exact as possible conditions.

The same procedure is adopted for the Hindmarsh-Rose equation and the resulting diagram is given in Fig. (20). Due to the more complicated nature of the equation it requires two TL084CN op-amps along with two multipliers AD633. The resistance and

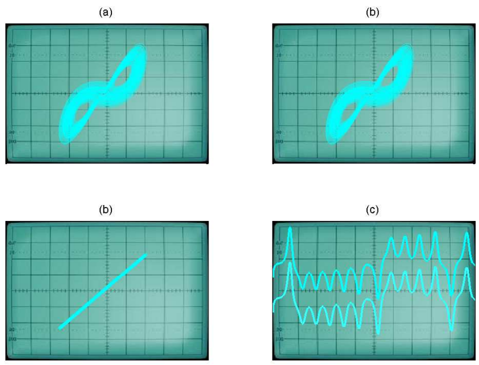

Figure 19: Oscilloscope pictures of Lorenz system at complete synchronization

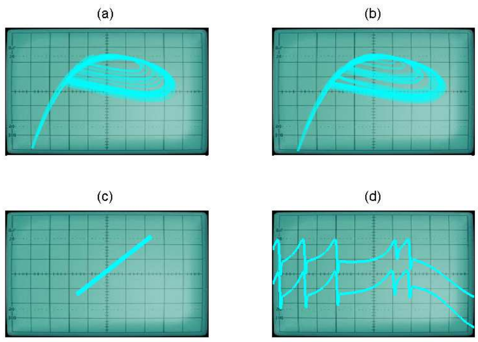

Figure 20: Oscilloscope pictures of Hindmarsh-Rose system at complete synchronization

capacitors are as usual. Along with the two sets for the two equations we have coupling circuit in middle of Fig. (18). For Hindmarsh-Rose electronic circuit[36, 37] we need to scale the variable to bring them within electronically active region of Op-amp. Scaling used for the present case is given as

$$u_{1,2} = x_{1,2},\ v_{1,2} = \frac{y_{1,2}}{3} \text{ and } w_{1,2} = z_{1,2}$$

The time scaling used for the electronic circuit is $T_s = 10^{-3} sec$. In the circuit, we have $I_{ref} = I$, $a = \frac{100k}{R_2}$, $b = \frac{300k}{R_7}$, $r = \frac{100k}{R_{17}}$ and $s = \frac{R_{15}}{R_{13}} = \frac{R_{15}}{R_{14}}$. The corresponding outputs can be observed in oscilloscope screen. These are given in Fig. (20). The two attractors are shown in Figs. (20a), (20b) where as the time series is given in (20d) and the synchronized signal appear in Fig. (20c). The whole arrangement is connected via one $NIUSB - 6363DAQ$ (32 AI Channels (16 BNC), 2 MS/s) to a computer to acquire the data generated by electronic circuit for further analysis. Here also circuits use resistance with 5% tolerance, a bit of trial and error goes before taking the actual data for bringing the two circuits to the exact as possible conditions.

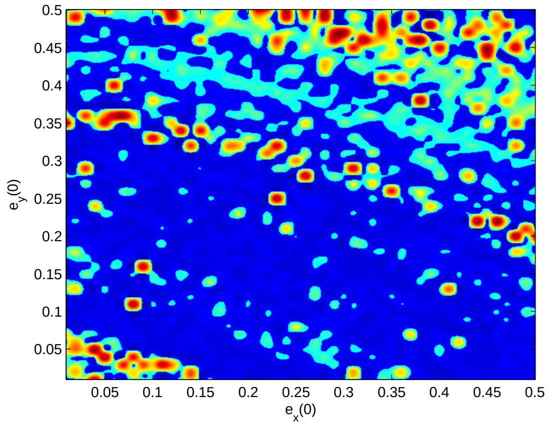

Figure 21: Initial difference region indicating complete synchronization of two Lorenz systems on $(e_x(0), e_y(0))$ plane. Figure is plotted for $c = 0.2$ Other parameter values are kept at $\sigma = 10,\ r = 28,\ \ b = \frac{8}{3}\ \alpha = 0.1$ and $\beta = 0.25$. Value of $e_z(0)$ is fixed at 0.1

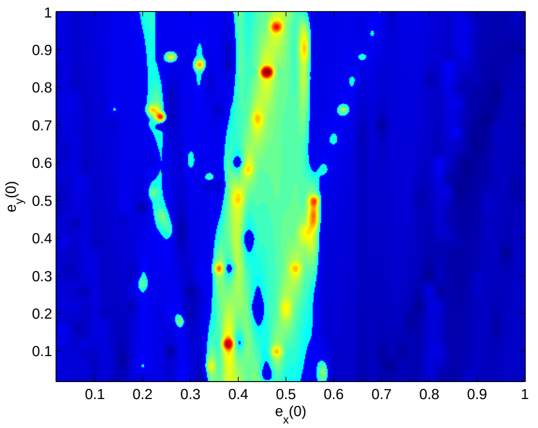

Figure 22: Initial difference region indicating complete synchronization of two Hindmarsh-Rose systems on $(e_x(0), e_y(0))$ plane. Figure is plotted for $c = 0.1.6$ Other parameter values are kept at $a = 3.0,\ b = 5.0,\ I = 3.05,\ s = 4.0,\ c_0 = 1.6$ and $r = 0.005,\ \alpha = 0.25$ and $\beta = 0.3$. Value of $e_z(0)$ is fixed at 0.1

4 Some observation

In our above analysis, we have seen two new aspects of synchronization phenomenon, when the two systems are coupled via memristor. The first one is the intermittency with respect to parameter variation. This is actually happening due to the generation of more than one attractor in the coupled system, though original Lorenz or Hindmarsh-Rose do not have such properties, To check this we have plotted the values of the Lyapunov exponents, against the values of the co-ordinates $(e_x(0), e_y(0))$ as in Fig. (21) and Fig. (22). One can visualize the extremely complicated nature of basin. Here we have shown synchronous region(with blue)and asynchronous region(with color ranging from light green to red) separately. On the other hand if we analyze the (u, x_1, y_1) projection of the attractor then an interesting phenomenon is seen. It is depicted in Fig. (23 a). Here we clearly see that we have a separate attractor as 'u'' changes. So, when we are analyzing the coupled system, there is a question of multiple attractor, and it is really responsible for the aforesaid intermittency. As expected the Hindmarsh-Rose system also have similar properties. Again from the plotting of the Lyapunov exponent values against $(e_x(0), e_y(0))$ we can see the complicated fractal basin structure, but the multiple attractor as 'u'' varies is shown in Fig. (23b). So the generation of multiple attractor dynamics is a novel output of the coupling via memristor, and which in turn is responsible for the whole phenomenon.

5 Conclusion

In our above analysis we have analyzed a different form of memristor coupling between two nonlinear oscillators and have observed a new type of intermittent synchronization. It is very interesting to note that the intermittency is occurring with respect to the parameter variation and also with the change of initial condition. This phenomena is actually a reflection of multi-attractor generation and a continuous transition from one attractor to another attractor. The situation has been studied both form the theoretical and experimental point of view. From analytical perspective, we could only study the local stability of the coupled system around the line fixed point. For the experimental part, we have used op-amp combination for the realization of memristor. Due to the memristor, the coupling is actually nonlinear. Recently, one of our colleague draw our attention to two papers where memristors are used to couple two chaotic systems[38, 39]. But they did not discuss the dependency of such system on initial conditional differences. This is where the present paper stands apart from those two papers. These type of events require more investigations to reveal its potentiality.

Acknowledgement: One of the authors, P. Saha is thankful to SERB (Department of Science and Technology, Govt of India) for a project (SR/FTP/PS-103/2012). A.Ray is grateful to CSIR (Council Of Scientific and Industrial Research, Govt. of India) for a Senior Research Fellowship and A. RoyChowdhury wishes to thank UGC (University Grants Commission, Govt. of India) for UGC-BSR one time grant which helped to upgrade the computational facility and for D S Kothari fellowship which made this work possible. D. C. Saha is grateful to UGC for a Minor Research Project.

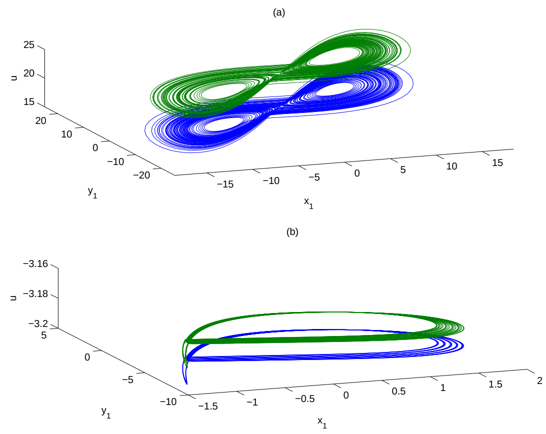

Figure 23: (a) Projection of Lorenz attractor on (x_1, y_1, u) plane when synchronization occures for two different combinations of $(e_x(0), e_y(0), e_z(0))$. Blue attractor is plotted for $(0.1, 0.1, 0.1)$ and green attractor is plotted with $(0.2, 0.1, 0.1)$. All other parameters are kept same as the previous values. (b) Projection of Hindmarsh-Rose attractor on (x_1, y_1, u) plane when synchronization occurs for two different combinations of $(e_x(0), e_y(0), e_z(0))$. All other parameters are kept same as the previous values. Blue attractor is plotted for $(0.1, 0.1, 0.1)$ and green attractor is plotted with $(0.2, 0.1, 0.1)$.

6 Appendix

6.1 Lorenz system

In Fig. (24), we have plotted the counter part of Fig. (8) of the main text. Like Fig. (8), this figure also depicts the variation of F_s with colors in (α, β) plane for different coupling strength ('c''). Here F_s denotes number (n_s) of combination of initial condition difference between coupled Lorenz system for which synchronization can be archived over total number (n) of such combinations taken for calculation(i.e., $F_s = \frac{n_s}{n}$). F_s values are depicted by different color regions and these are stated in colormap diagram on right side of the figure. We have also calculated detail variations of F_s for coupled system of Lorenz equations on (α, β) plane for different values of coupling c. As evident from Fig. (24), there is an anomalous behavior in variation of F_s in (α, β) plane with variation of 'c. If we follow the figure, we can see that maximum value of F_s (reprsented with red color lines and region) defines an island like structure and travels from top to bottom on left hand side of these figures.

6.2 Hindmarsh-Rose system

In Fig. (25), we have plotted the counter part of Fig. (13) of the main text. Like Fig. (13), this figure also depicts the variation of F_s with colors in (α, β) plane for different coupling strength('c''). Here F_s denotes number(n_s) of combination of initial condition difference between coupled Hindmarsh-Rose system for which synchronization can be archived over total number (n) of such combinations taken for calculation(i.e., $F_s = \frac{n_s}{n}$). F_c values are

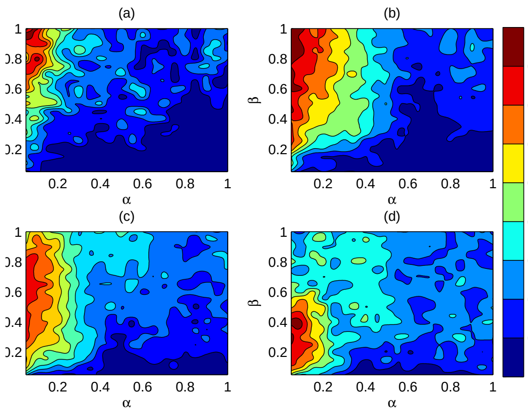

Figure 24: Parameter region indicating fraction(F_c) of different initial condition difference combination that reaches synchronization for a particular value of coupling 'c' on (α, β) plane. Fig. (a) is plotted for $c = 0.3$, Fig. (b) is plotted for $c = 0.6$, Fig. (c) is plotted for $c = 0.8$ and Fig. (d) is plotted for $c = 1.0$. Other parameter values are kept at $\sigma = 10,\ r = 28$ and $b = \frac{8}{3}$.

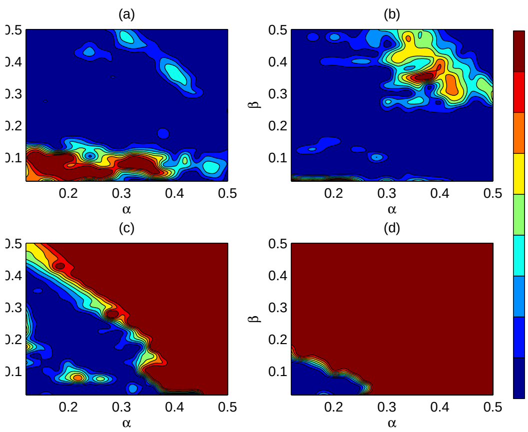

Figure 25: Parameter region indicating fraction (F_s) of different initial condition difference combination that reaches synchronization for a particular value of coupling 'c' on (α, β) plane. Fig. (a) is plotted for $c = 0.2$, Fig. (b) is plotted for $c = 0.3$, Fig. (c) is plotted for $c = 0.5$ and Fig. (d) is plotted for $c = 0.7$. Other parameter values are kept at $a = 3.0,\ b = 5.0,\ I = 3.05,\ s = 4.0,\ c_0 = 1.6\ \ r = 0.005,$ and $\alpha = 0.1$.

depicted by different color regions and these are stated in colormap diagram on right side of the figure. Then, we have plotted the fraction F_s of coupled Hindmarsh-Rose neurons on (α, β) plane for different values of coupling c. Here color varies between red and blue though green. Red denotes fraction value near to '$0.9'$ where as that of blue represents fraction value near to '$0.0'$. Also green denotes fraction value near to '$0.5'$. As evident from Fig. (25), there is also an anomalous behavior in variation of F_s in (α, β) plane with variation of 'c. If we follow the figure, we can see that maximum value of F_s (reprsented with red color lines and region) defines an island like structure and travels from bottom to top diagonally in these figures. Initially value of F_s is high for lower range of (α, β). As 'c' is increased beyond the value 0.6, F_s is high for higher range of (α, β).

References

[1] L.O. Chua. Memristor-the missing circuit element. *Circuit Theory, IEEE Transactions on*, 18(5):507–519, Sep 1971.

[2] L.O. Chua and Sung Mo Kang. Memristive devices and systems. *Proceedings of the IEEE*, 64(2):209–223, Feb 1976.

[3] Dmitri B. Strukov, Gregory S. Snider, Duncan R. Stewart, and R. Stanley Williams. The missing memristor found. *Nature*, 453(7191):80–83, May 2008.

[4] Sieu D. Ha and Shriram Ramanathan. Adaptive oxide electronics: A review. *Journal of Applied Physics*, 110(7):–, 2011.

[5] Suresh Chandra. On the discovery of a polarity-dependent memory switch and/or memristor (memory resistor). *IETE Technical Review*, 27(2):179–180, 2010.

[6] Yuriy V. Pershin and Massimiliano Di Ventra. Experimental demonstration of associative memory with memristive neural networks. *Neural Netw.*, 23(7):881–886, September 2010.

[7] Yuriy V. Pershin and Massimiliano Di Ventra. Practical approach to programmable analog circuits with memristors. *Trans. Cir. Sys. Part I*, 57(8):1857–1864, August 2010.

[8] Makoto Itoh and Leon O. Chua. Memristor oscillators. *International Journal of Bifurcation and Chaos*, 18(11):3183–3206, 2008.

[9] Bharathwaj Muthuswamy. Implementing memristor based chaotic circuits. *International Journal of Bifurcation and Chaos*, 20(05):1335–1350, 2010.

[10] Arturo Buscarino, Luigi Fortuna, Mattia Frasca, and Lucia Valentina Gambuzza. A gallery of chaotic oscillators based on hp memristor. *International Journal of Bifurcation and Chaos*, 23(05):1330015, 2013.

[11] Gerard David Howard, Larry Bull, Ben De Lacy Costello, Andrew Adamatzky, and Victor Erokhin. A spice model of the peo-pani memristor. *International Journal of Bifurcation and Chaos*, 23(06):1350112, 2013.

[12] Junwei Sun, Yi Shen, Quan Yin, and Chengjie Xu. Compound synchronization of four memristor chaotic oscillator systems and secure communication. *Chaos: An Interdisciplinary Journal of Nonlinear Science*, 23(1):–, 2013.

[13] Don Monroe. Neuromorphic computing gets ready for the (really) big time. *Commun. ACM*, 57(6):13–15, June 2014.

[14] W S Zhao, G Agnus, V Derycke, A Filoramo, J-P Bourgoin, and C Gamrat. Nanotube devices based crossbar architecture: toward neuromorphic computing. *Nanotechnology*, 21(17):175202, 2010.

[15] Mrigank Sharad, Charles Augustine, Georgios Panagopoulos, and Kaushik Roy. Proposal for neuromorphic hardware using spin devices. *CoRR*, abs/1206.3227, 2012.

[16] Matthew D. Pickett, Gilberto Medeiros-Ribeiro, and R. Stanley Williams. A scalable neuristor built with Mott memristors. *Nature materials*, 2012.

[17] Matthew D Pickett and R Stanley Williams. Phase transitions enable computational universality in neuristor-based cellular automata. *Nanotechnology*, 24(38):384002, 2013.

[18] Arkady Pikovsky, Michael Rosenblum, and Jürgen Kurths. *Synchronization*. Cambridge University Press, 2001. and the references therein.

[19] G.V. Osipov, J. Kurths, and C. Zhou. *Synchronization in Oscillatory Networks*. Springer Series in Synergetics. Springer, 2007. and the references therein.

[20] K. S. Thornburg, M. Möller, Rajarshi Roy, T. W. Carr, R.-D. Li, and T. Erneux. Chaos and coherence in coupled lasers. *Phys. Rev. E*, 55:3865–3869, Apr 1997.

[21] Peter Ashwin, John R. Terry, K. Scott Thornburg, and Rajarshi Roy. Blowout bifurcation in a system of coupled chaotic lasers. *Phys. Rev. E*, 58:7186–7189, Dec 1998.

[22] István Z. Kiss, Vilmos Gáspár, and John L. Hudson. Experiments on synchronization and control of chaos on coupled electrochemical oscillators. *The Journal of Physical Chemistry B*, 104(31):7554–7560, 2000.

[23] C. Masoller, Hugo L. D. de S. Cavalcante, and J. R. Rios Leite. Delayed coupling of logistic maps. *Phys. Rev. E*, 64:037202, Aug 2001.

[24] Mary Ann Harrison, Ying-Cheng Lai, and Robert D. Holt. Dynamical mechanism for coexistence of dispersing species without trade-offs in spatially extended ecological systems. *Phys. Rev. E*, 63:051905, Apr 2001.

[25] L. Glass. Synchronization and rhythmic processes in physiology. *Nature*, 410(6825):277–284, March 2001.

[26] Juan A. Acebrón, L. L. Bonilla, Conrad J. Pérez Vicente, Félix Ritort, and Renato Spigler. The kuramoto model: A simple paradigm for synchronization phenomena. *Rev. Mod. Phys.*, 77:137–185, Apr 2005.

[27] A.J. Koch and H. Meinhardt. Biological pattern formation: from basic mechanisms to complex structures. *Rev. Mod. Phys.*, 66:1481–1507, 1994.

[28] RenatoE. Mirollo and StevenH. Strogatz. Amplitude death in an array of limit-cycle oscillators. *Journal of Statistical Physics*, 60(1-2):245–262, 1990.

[29] D. G. Aronson, G. B. Ermentrout, and N. Kopell. Amplitude response of coupled oscillators. *Phys. D*, 41(3):403–449, April 1990.

[30] D. V. Ramana Reddy, A. Sen, and G. L. Johnston. Time delay induced death in coupled limit cycle oscillators. *Phys. Rev. Lett.*, 80:5109–5112, Jun 1998.

[31] Aneta Koseska, Evgenii Volkov, and Jürgen Kurths. Oscillation quenching mechanisms: Amplitude vs. oscillation death. *Physics Reports*, 531(4):173 – 199, 2013. Oscillation quenching mechanisms: Amplitude vs. oscillation death.

[32] Edward N. Lorenz. Deterministic Nonperiodic Flow. *J. Atmos. Sci.*, 20(2):130–141, March 1963.

[33] J. L. Hindmarsh and R. M. Rose. A model of neuronal bursting using three coupled first order differential equations. *Proceedings of the Royal Society of London B: Biological Sciences*, 221(1222):87–102, 1984.

[34] Michael Rosenblum, Arkady Pikovsky, and Jürgen Kurths. Phase synchronization of chaotic oscillators. *Phys. Rev. Lett.*, 76:1804–1807, Mar 1996.

[35] Jonathan N. Blakely, Michael B. Eskridge, and Ned J. Corron. A simple lorenz circuit and its radio frequency implementation. *Chaos: An Interdisciplinary Journal of Nonlinear Science*, 17(2):–, 2007.

[36] Young Jun Lee, Jihyun Lee, Kyung Ki Kim, Yong-Bin Kim, and Joseph Ayers. Low power cmos electronic central pattern generator design for a biomimetic underwater robot. *Neurocomputing*, 71(13):284 – 296, 2007. Dedicated Hardware Architectures for Intelligent Systems Advances on Neural Networks for Speech and Audio Processing.

[37] R. Pinto, P. Varona, A. Volkovskii, A. Szücs, Henry Abarbanel, and M. Rabinovich. Synchronous behavior of two coupled electronic neurons. *Phys. Rev. E*, 62:2644–2656, Aug 2000.

[38] F. Corinto, A. Ascoli, V. Lanza, and M. Gilli. Memristor synaptic dynamics' influence on synchronous behavior of two hindmarsh-rose neurons. In *Neural Networks (IJCNN), The 2011 International Joint Conference on*, pages 2403–2408, July 2011.

[39] Mattia Frasca, Lucia Valentina Gambuzza, Arturo Buscarino, and Luigi Fortuna. Implementation of adaptive coupling through memristor. *physica status solidi (c)*, 12 (1-2): 206–210, 2015.